

# Syngas Production Via High-Temperature Co-electrolysis of Steam and Carbon Dioxide in a Solid-Oxide Stack

**Fuel Cell Science, Engineering & Technology Conference**

Carl M. Stoots  
James E. O'Brien  
Joseph J. Hartvigsen

June 2007

The INL is a  
U.S. Department of Energy  
National Laboratory  
operated by  
Battelle Energy Alliance



This is a preprint of a paper intended for publication in a journal or proceedings. Since changes may be made before publication, this preprint should not be cited or reproduced without permission of the author. This document was prepared as an account of work sponsored by an agency of the United States Government. Neither the United States Government nor any agency thereof, or any of their employees, makes any warranty, expressed or implied, or assumes any legal liability or responsibility for any third party's use, or the results of such use, of any information, apparatus, product or process disclosed in this report, or represents that its use by such third party would not infringe privately owned rights. The views expressed in this paper are not necessarily those of the United States Government or the sponsoring agency.

**SYNGAS PRODUCTION VIA HIGH-TEMPERATURE COELECTROLYSIS OF STEAM AND CARBON  
DIOXIDE IN A SOLID-OXIDE STACK**

Carl M. Stoots, James E. O'Brien

*Idaho National Laboratory  
Idaho Falls, Idaho 83415-3890  
carl.stoots@inl.gov*

Joseph J. Hartvigsen

*Ceramatec, Inc.  
Salt Lake City, UT 84119  
jjh@ceramatec.com*

**ABSTRACT**

This paper presents results of recent experiments conducted at the INL studying coelectrolysis of steam and carbon dioxide in a 10-cell high-temperature solid-oxide electrolysis stack. Coelectrolysis is complicated by the fact that the reverse shift reaction occurs concurrently with the electrolytic reduction reactions. All reactions must be properly accounted for when evaluating results. Electrochemical performance of the stack was evaluated over a range of temperatures, compositions, and flow rates. The apparatus used for these tests is heavily instrumented, with precision mass-flow controllers, on-line dewpoint and CO<sub>2</sub> sensors, and numerous pressure and temperature measurement stations. It also includes a gas chromatograph for analyzing outlet gas compositions. Comparisons of measured compositions to predictions obtained from a chemical equilibrium co-electrolysis model are presented, along with corresponding polarization curves. Results indicate excellent agreement between predicted and measured outlet compositions. Coelectrolysis significantly increases the yield of syngas over the reverse water gas shift reaction equilibrium composition. The process appears to be a promising technique for large-scale syngas production.

## I. INTRODUCTION

It is anticipated that world oil production will peak within the next few decades, in spite of the fact that the worldwide demand for light hydrocarbon fuels like gasoline and diesel oil continues to increase. The burning of these fuels results in significant greenhouse gas emissions and contributes to global warming. Therefore, two of the top energy priorities for the United States are finding environmentally friendly alternatives to fossil fuels and reducing/eliminating anthropogenic carbon dioxide emissions.

For the long term, the United States is exploring the feasibility of a hydrogen-based energy economy, with the goals of reduced oil consumption, foreign energy independence, and reduced greenhouse gas emissions. However, since hydrogen is an energy carrier and not an energy source, attaining these goals is conditional upon development of suitable renewable energy sources and/or nuclear power. Furthermore, the conversion process to a hydrogen-based energy economy will require decades due to the already existing tremendous infrastructure based upon liquid hydrocarbons.

An interim solution and a bridge to a hydrogen economy are synthetically-derived hydrocarbon fuels (synfuels). While at present synfuels are produced mostly because of subsidies, synfuel production is a mature technology. The raw material for synfuel production is syngas – a mixture of hydrogen ( $H_2$ ) and carbon monoxide (CO). Traditionally, syngas has been produced via coal gasification, and more recently by steam reforming of natural gas. Both techniques consume non-renewables and emit green-house gases.

For the past several years, the Idaho National Laboratory (INL) has had an on-going project funded by the Department of Energy (DOE) under the Nuclear Hydrogen Initiative (NHI) studying nuclear-powered high-temperature electrolysis of steam using solid-oxide cells for large-scale hydrogen production. Complementary to this research, the INL, in conjunction with Ceramatec Inc. (Salt Lake City, USA), has also been researching the use of solid oxide cells for simultaneous electrolysis (co-electrolysis) of steam/ $CO_2$  mixtures to produce syngas (Refs. 1, 2):



When linked to a nuclear power source, this technology provides a feedstock for synfuel production without the consumption of fossil fuels and without emitting green-house gases.

Co-electrolysis not only entails the reduction of steam and  $CO_2$ , but also the reverse shift reaction (RSR):



Reaction kinetics govern the relative contributions of these three reactions. It is also important to note that the electrolysis reactions are not equilibrium reactions. The electrolyte separates the products from the reactants. However, the RSR is a kinetically fast, equilibrium reaction at high temperature in the presence of a Ni catalyst. Also, if the cell potential is high enough, CO can be further electrolyzed to elemental C:



which can then deposit on cell surfaces and reduce cell performance. At temperatures below 700°C, catalytic (Ni) formation of methane may occur (Refs. 3, 4):



Finally, there could be material compatibility issues related to corrosion and seal leakage.

Steam and CO<sub>2</sub> could be electrolyzed separately to produce syngas, avoiding some of the above complexity. There are, however, significant advantages to electrolyzing steam and CO<sub>2</sub> simultaneously. Focusing only upon the electrolysis step, coelectrolysis is more energy efficient than separate electrolysis. For a given solid oxide electrolysis cell, CO<sub>2</sub> electrolysis will exhibit a higher area specific resistance (ASR) than for steam electrolysis. This is due to the slower overall kinetics of CO<sub>2</sub> electrolysis and the higher overpotentials required. In coelectrolysis, the reverse gas shift reaction is relied upon for most of the CO production and therefore the overall electrical requirement is less. A second advantage is that in coelectrolysis the likelihood of producing carbon by electrolysis of CO is reduced.

Results of CO<sub>2</sub>/H<sub>2</sub>O electrolysis experiments performed to date in a 10-cell planar solid oxide stack are presented and discussed. These results include electrolysis performance at various temperatures, gas mixtures, and electrical settings. Product gas compositions, as measured via an online micro gas chromatograph (GC), are compared to predictions obtained from a chemical equilibrium/electrolysis model. Better understanding of the feasibility of producing syngas using high temperature electrolysis may initiate the systematic investigation of nuclear-powered synfuel production as a bridge to the future hydrogen economy and ultimate independence from foreign energy resources (Ref. 4).

## II. DESCRIPTION OF TEST FACILITY

A schematic of the apparatus used for co-electrolysis testing at the INL is shown in Fig. 1. A photograph of the test hardware follows in Fig. 2. Primary components include gas supply cylinders, mass-flow controllers, a humidifier, dewpoint

measurement stations, carbon dioxide concentration measurement stations, microchannel gas chromatograph, temperature and pressure measurement, high temperature furnace, and a solid oxide electrolysis cell. Nitrogen is used as an inert carrier gas. The use of a carrier gas allows for independent variation of both the partial pressures and the flow rates of the inlet steam, hydrogen, and CO<sub>2</sub> gases with operation near atmospheric pressure. The flow rates of nitrogen, hydrogen and air are established by means of precision mass-flow controllers. Air flow to the stack is supplied by the shop air system, after passing through a two-stage extractor / dryer unit.

Downstream of the mass-flow controllers, nitrogen is mixed with smaller flows of hydrogen gas and CO<sub>2</sub>. Hydrogen is included in the inlet flow as a reducing gas in order to prevent oxidation of the nickel cermet electrode material. The nitrogen / hydrogen / CO<sub>2</sub> gas mixture is mixed with steam by means of a heated humidifier. The humidifier water temperature is maintained at a constant setpoint value using computerized feedback control. The dewpoint temperature of the nitrogen / hydrogen / CO<sub>2</sub> / steam gas mixture exiting the humidifier is monitored continuously using a precision dewpoint sensor. Pressure is also measured at the dewpoint measurement stations using absolute pressure transducers. Local stream pressure

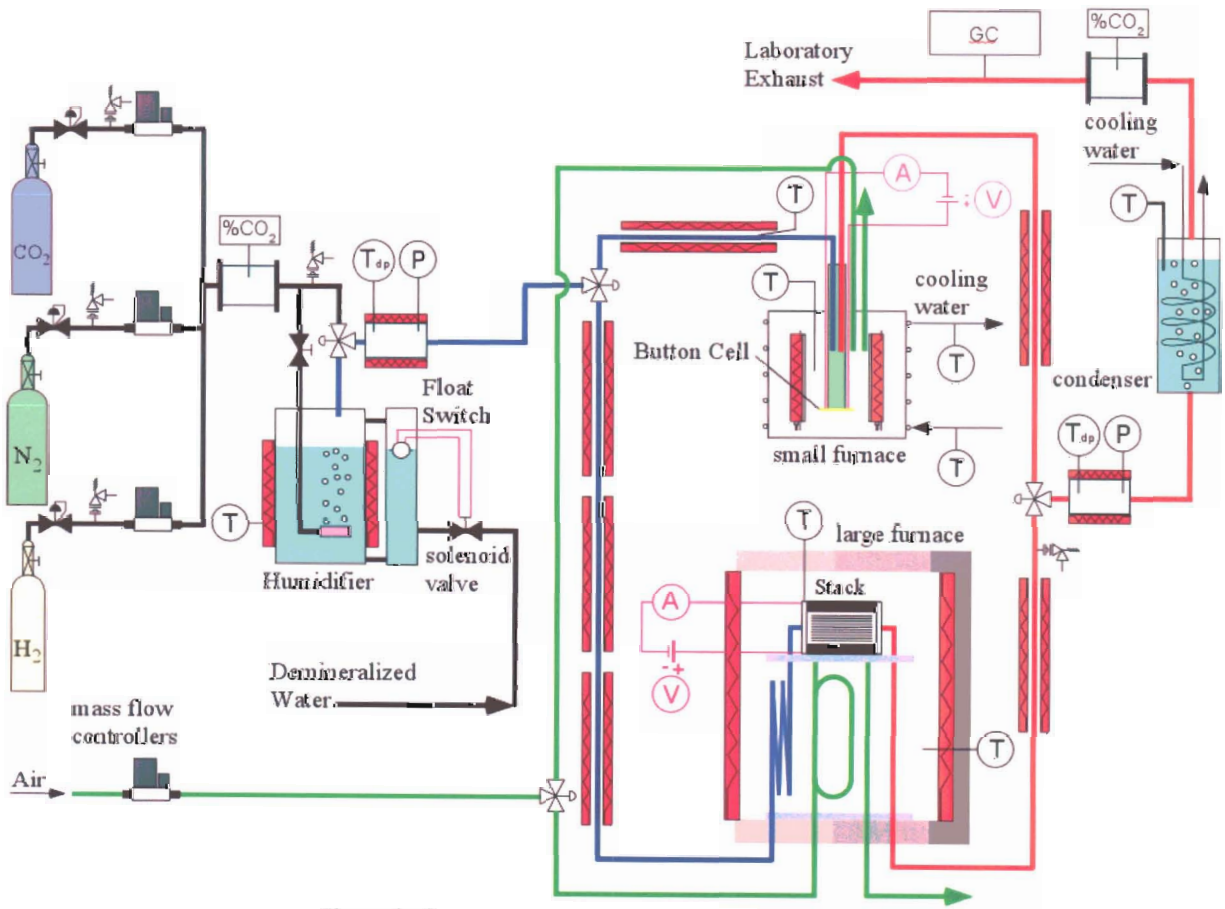


Figure 1. Schematic of INL coelectrolysis test apparatus.



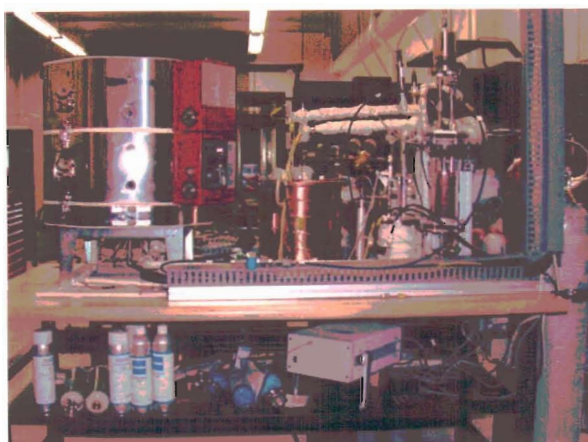


Figure 2. Photograph of the INL coelectrolysis apparatus.

information is required to determine the mole fraction of steam in the gas mixture at the dew point measurement station. These measurements have indicated that the dewpoint temperature of the gas mixture leaving the humidifier is very close to the water bath temperature, but not necessarily equal to it. Inlet  $\text{CO}_2$  concentration is also monitored using an infrared  $\text{CO}_2$  sensor. Since the vapor pressure of the water and the resulting partial pressure of the steam exiting the humidifier are determined by the water bath temperature, the water vapor mass flow rate is directly proportional to the carrier gas flow rate for a specified bath temperature. Also, since the nitrogen, hydrogen, and  $\text{CO}_2$  flow rates are fixed by the mass flow controllers, and the steam partial pressure is fixed by the bath temperature, the complete inlet gas composition is precisely known at all times. All gas lines located downstream of the humidifier are heat-traced in order to prevent steam condensation. Gas line temperatures are monitored by thermocouples and controlled by means of computer-controlled SCRs.

The inlet gas mixture is then directed to the high temperature furnace (Skutt Model KS818-3), capable of producing temperatures up to  $1250^\circ\text{C}$ , which heats and maintains the electrolyzer at the appropriate test temperature via computer-based feedback control. The furnace also preheats the inlet gas mixture and the air sweep gas. A photograph of the stack, mounted on its inconel test fixture and resting on the furnace base, is shown in Fig. 3. The power leads are inconel rods insulated with alumina tubing. The steam /hydrogen /  $\text{CO}_2$  and air sweep inlet tubes are coiled to provide additional length for heat transfer upstream of the stack. Coelectrolysis testing was performed in the temperature range of  $800\text{--}830^\circ\text{C}$ .

The stack was fabricated by Ceramatec, Inc., of Salt Lake City, UT. This stack has a per-cell active area of  $64\text{ cm}^2$ , for a total active area of  $640\text{ cm}^2$ . It is designed to operate in cross flow, with the steam /hydrogen /  $\text{CO}_2$  gas mixture entering the inlet manifold on the right side in the photograph (Fig. 3), and exiting through the outlet manifold, visible on the left (Fig. 3). Airflow enters at the rear through an air inlet manifold, not visible in Fig. 3, and exits at the front directly into the furnace.



Figure 3. 10-cell stack mounted on test fixture on furnace base, ready to test.

Fig. 4 is a close-up of the 10-cell stack air outlet plane, showing the miniature intra-cell thermocouples, voltage taps, and power lead bus bars. The power lead attachment tabs are integral with the upper and lower interconnect plates. Stack operating voltages were measured using wires that were directly spot-welded onto these tabs. Four intermediate cell voltages were monitored using small diameter wires inserted into the airflow channels. In addition, two miniature thermocouples were inserted into the airflow channels to monitor internal stack temperatures. These were inconel-sheathed, 0.020 in. (500  $\mu\text{m}$ ) OD, mineral-insulated, ungrounded, type-K thermocouples. Thermocouple #1 was located centrally on the top cell (cell #1) and thermocouple #2 was located centrally on the sixth cell from the top.

The internal components of the stack are comprised as follows. The interconnect plate is fabricated primarily from ferritic stainless steel. It includes an impermeable separator plate (~0.46 mm thick) with edge rails and two corrugated “flow fields,” one on the sweep-gas side and one on the steam / hydrogen /  $\text{CO}_2$  side. The height of the flow channel formed by the edge rails and flow fields is 1.0 mm. Each flow field includes 32 perforated flow channels across its width to provide uniform gas-flow distribution. The steam / hydrogen /  $\text{CO}_2$  flow field is fabricated from nickel foil. The sweep flow field is ferritic stainless steel. The interconnect plates and flow fields also serve as electrical conductors and current distributors. To improve performance, the sweep-side separator plates and flow fields are surface - treated to form a rare-earth conductive

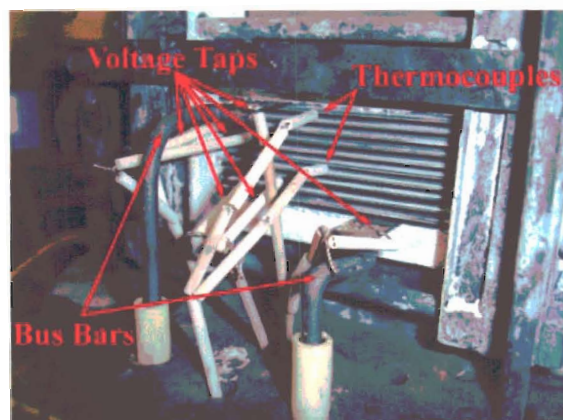


Figure 4. Close-up of 10-cell stack, showing intra-cell thermocouples, voltage leads, and power leads.

oxide scale. A perovskite rare-earth coating is also applied to the separator-plate oxide scale by either screen printing or plasma spraying. On the steam / hydrogen / CO<sub>2</sub> side of the separator plate, a thin (~10 μm) nickel metal coating is applied.

The electrolyte is scandia-stabilized zirconia, ~140 μm thick. The sweep-side electrode (anode in the electrolysis mode) is a strontium-doped manganite. The electrode is graded, with an inner layer of manganite/zirconia (~13 μm) immediately adjacent to the electrolyte, a middle layer of manganite (~18 μm), and an outer bond layer of cobaltite. The steam / hydrogen / CO<sub>2</sub> electrode (cathode in the electrolysis mode) is also graded, with a nickel cermet layer (~13 μm) immediately adjacent to the electrolyte and a pure nickel outer layer (~10 μm).

The syngas product stream exiting the furnace is directed towards a second dewpoint sensor and a CO<sub>2</sub> sensor upon exiting the furnace and then to a condenser through a heat-traced line. The condenser removes most of the residual steam from the exhaust. The final exhaust stream is vented outside the laboratory through the roof.

The rates of steam and CO<sub>2</sub> electrolysis are measured via three different, independent methods: 1) electrical current through the stack, 2) the measured change in inlet and outlet steam and CO<sub>2</sub> concentrations as measured by the on-line dew point and CO<sub>2</sub> sensors, and 3) an on-line microchannel GC. The GC also tests for any additional electrolysis products, such as CH<sub>4</sub>, that may be produced.

Some additional discussion of the test apparatus, experimental procedures, data reduction, and the stack construction may be found in Ref. 5.

### III. DESCRIPTION OF MODEL

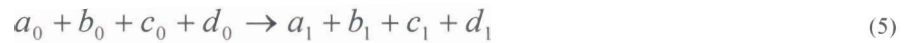
To understand the impact of the electrolysis reactions and the RSR discussed above, and to assist with interpretation of experimentally measured data, a chemical equilibrium coelectrolysis model was developed. This model also served to help



determine the necessary inlet conditions for the range of experiments that were conducted. A description of the INL-developed model follows.

The open-cell potential for the coelectrolysis system can be calculated as a function of temperature using the Nernst equation for either steam-hydrogen or for CO<sub>2</sub>-CO, provided the equilibrium composition of the components is used in the evaluating the equation. Therefore, the equilibrium composition must be determined first, by any appropriate method. Using a correlation for the RSR equilibrium constant as a function of gas temperature and the room temperature inlet gas molar composition, the model first calculates the equilibrium gas composition as the inlet gas mixture heats up to electrolysis conditions (800 to 830°C), and then the model accounts for the electrolysis reactions and RSR at process conditions.

The overall shift reaction can be represented as:



where  $a_0$ ,  $b_0$ ,  $c_0$ , and  $d_0$  represent the cold inlet mole fractions of CO, CO<sub>2</sub>, H<sub>2</sub>, and H<sub>2</sub>O, respectively, that are known from the inlet gas flow rate and dewpoint measurements. The unknown equilibrium mole fractions of the four species at the electrolyzer temperature, prior to electrolysis, are represented by  $a_1$ ,  $b_1$ ,  $c_1$ , and  $d_1$ . The three corresponding chemical balance equations for carbon, hydrogen, and oxygen are:

$$a_0 + b_0 = a_1 + b_1 \quad (6)$$

$$2c_0 + 2d_0 = 2c_1 + 2d_1 \quad (7)$$

$$a_0 + 2b_0 + d_0 = a_1 + 2b_1 + d_1. \quad (8)$$

To complete a system of four equations and four unknowns, the equilibrium constant for the shift reaction:

$$k_{RSR}(T) = \frac{b_1 c_1}{a_1 d_1} \quad (9)$$

is included.

Once the hot equilibrium composition is determined, the Nernst potential can be calculated from:

$$\begin{aligned}
V_N &= \frac{-\Delta G_{f,H_2O}(T)}{2F} - \frac{RT}{2F} \ln \left[ \left( \frac{d_1}{c_1 y_{O_2}^{1/2}} \right) \left( \frac{P}{P_{std}} \right)^{-1/2} \right] \\
&= \frac{-\Delta G_{f,CO_2}(T)}{2F} - \frac{RT}{2F} \ln \left[ \left( \frac{d_1}{c_1 y_{O_2}^{1/2}} \right) \left( \frac{P}{P_{std}} \right)^{-1/2} \right]
\end{aligned} \tag{10}$$

where  $\Delta G_{f,H_2O}$  and  $\Delta G_{f,CO_2}$  are the Gibbs free energy of formation for H<sub>2</sub>O and CO<sub>2</sub>,  $R$  is the ideal gas constant, and  $y_{O_2}$  is the mole fraction of oxygen on the sweep side of the cells ( $y_{O_2} \sim 0.21$ ).

The electrolyzer outlet composition can be determined similarly, with one exception. The chemical balance equation for oxygen must be modified to account for the electrolytic reduction of the CO<sub>2</sub>/steam mixture. Accordingly, the oxygen balance equation becomes:

$$a_1 + 2b_1 + d_1 = a_2 + 2b_2 + d_2 + \Delta n_O \tag{11}$$

where  $\Delta n_O$  is the relative molar rate of oxygen removal from the CO<sub>2</sub> / steam mixture, give by:

$$\Delta n_O = \frac{IN_{cells}}{2F\dot{N}_{Tot, fuel}} \tag{12}$$

In this equation,  $I$  is the electronic current,  $N_{cells}$  is the total number of cells in the stack, and  $\dot{N}_{Tot, fuel}$  is the total molar flow rate on the CO<sub>2</sub>/steam side, including any inert gas flows. So the post-electrolyzer equilibrium composition (state 2) can be determined again from simultaneous solution of three chemical balance equations and the equilibrium constant equation.

The model was verified by comparing results with experimental results for various electrolysis current values, inlet compositions, and electrolysis temperatures.

#### IV. DISCUSSION OF RESULTS

Prior to testing a multi-cell stack under coelectrolysis conditions, many small button cells (single cells of approximately 2.5 cm<sup>2</sup> active area) were tested and used to verify the above model. The success of these earlier tests prompted INL researchers to test a 10-cell stack (Figs. 3 and 4) under coelectrolysis conditions in part to assess the feasibility of high temperature co-electrolysis for syngas production, as well as test the accuracy of the coelectrolysis chemical equilibrium model. Several different sets of inlet compositions and operating temperatures were studied (Table 1).

TABLE 1. Summary of test conditions.

Test #	T <sub>furnace</sub> (C)	Flow Rates			Inlet Dew Point (C)	Molar Composition			
		H <sub>2</sub> (sccm)	CO <sub>2</sub> (sccm)	N <sub>2</sub> (sccm)		H <sub>2</sub> (mol %)	CO <sub>2</sub> (mol %)	N <sub>2</sub> (mol %)	H <sub>2</sub> O (mol %)
0	800	497	0	3010	51.5	12.0	0	72.6	15.4
1	800	497	605	3010	51.5	10.2	12.4	61.9	15.5
2	800	497	505	2510	45.5	12.6	12.7	63.3	11.4
3	800	497	705	1010	66.0	15.6	22.2	31.8	30.4
4	800	497	756	3010	74.0	6.7	10.1	40.2	43.0
5	828	497	605	3011	51.5	10.2	12.4	61.9	15.5
6	828	497	756	3513	65.3	7.3	11.2	52.0	29.5

The stack was heated slowly overnight (2.25 C/min) with a gas flow of 3000 sccm N<sub>2</sub> flow rate, 497 sccm H<sub>2</sub> flow rate, and an inlet gas dew point temperature of 51.8 C. No CO<sub>2</sub> was introduced during heat up. Figure 5 shows the heat-up profile for the stack. The stack does not exhibit an open cell potential (OCV) until above approximately 300-350 C, at which point the electrolyte becomes an ion conductor. The orange line represents the theoretical Nernst potential for the gas mixture, agreeing quite well with the measured stack OCV. The outlet dew point temperature remains constant since there is no RSR or electrolysis reaction occurring.

Cell ASR is a measure of total electrical resistance and is comprised of ohmic resistances, contact resistances, and ionic resistances. The ASR is dependent upon the type of electrolysis being conducted, with pure CO<sub>2</sub> electrolysis exhibiting a significantly higher ASR than steam electrolysis (Ref. 1). However, in coelectrolysis the RSR is relied upon for most CO<sub>2</sub>-to-CO conversion, and steam electrolysis is the primary electrolytic reaction. Therefore, there is little change in ASR from steam electrolysis to coelectrolysis. To demonstrate this, polarization curves were generated for the 10-cell stack for steam

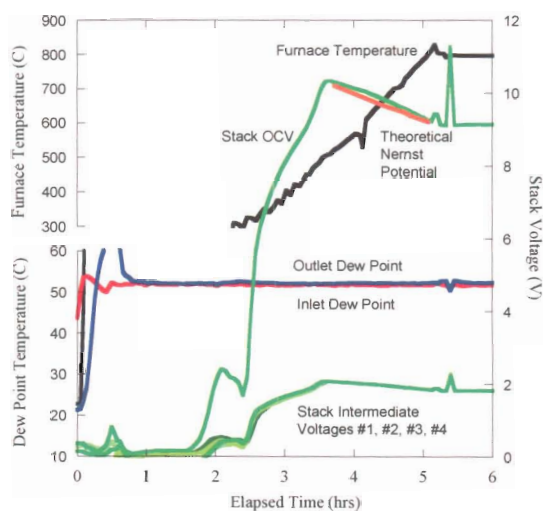


Figure 5. Heat-up results for stack #1.

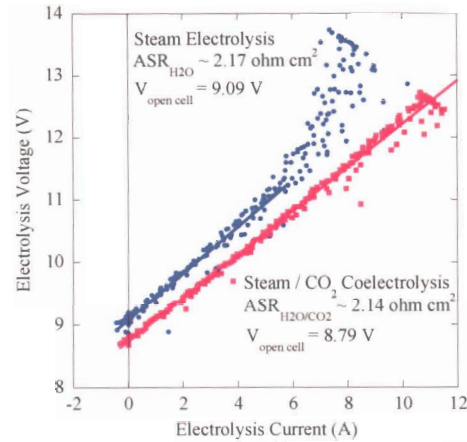


Figure 6. Polarization curves for steam electrolysis and coelectrolysis, with mean ASR values.

electrolysis and H<sub>2</sub>O/CO<sub>2</sub> coelectrolysis. Once the stack was at the operating temperature of 800°C, a steam electrolysis polarization curve was generated by performing a voltage sweep for the conditions labeled “Test #0” in Table 1. This same voltage sweep was repeated for the coelectrolysis conditions “Test #1”. These results are shown in Figure 6. Using these data, the sweep-average apparent ASR was calculated by numerically averaging the voltage and current data:

$$ASR = \sum \frac{1}{n} \frac{(V_{op} - V_{OC}) / N_{cells}}{I / A_{cell}} \quad (13)$$

where  $n$  is the number of measurements included,  $V_{op}$  is the operating voltage,  $V_{oc}$  is the measured open cell potential, and  $A_{cell}$  is the active area of each cell (64 cm<sup>2</sup>). Steam electrolysis sweep data above 6 A current exhibited a large amount of scatter, possibly due to local steam starvation, and was not included in the apparent ASR calculations. The straight lines represent linear fits of the data. There was almost no change in apparent ASR for coelectrolysis versus steam electrolysis,

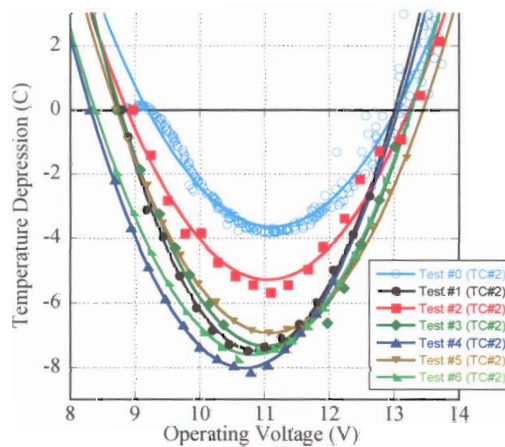


Figure 7. Internal stack temperature (thermocouple #2) for various test conditions.



reinforcing the hypothesis that steam electrolysis is the principal electrolysis reaction and that the RSR is mostly responsible for CO production.

Tests 1 through 6 comprised very slow voltage sweeps where for each power supply voltage setting the stack was allowed to reach thermal and chemical equilibrium. Thermal equilibrium was determined by watching the response of the stack internal thermocouples. Chemical equilibrium was recognized when the downstream dew point reading reached steady state. These two conditions were usually met after approximately 10 minutes at each setting.

When a solid oxide cell is operated as a fuel cell, the exothermic heat of reaction as well as ohmic heating tends to increase the cell temperature and cooling is required. Steam electrolysis, CO<sub>2</sub> electrolysis, as well as the RSR, however, are endothermic reactions which tend to reduce the cell temperature in proportion to the electrolysis current. Ohmic heating is proportional to the square of the electrolysis current. These two effects balance each other at the thermal neutral voltage. At operating voltages below thermal neutral, the endothermic heat of reaction dominates and the cell temperature is lower than that at open cell. At operating voltages above thermal neutral, ohmic heating dominates and the cell temperature will exceed that at open cell. For pure steam electrolysis, the thermal neutral voltage is a weak function of temperature only and is equal to 1.287 V at 800°C and 1.288 V at 830°C. For coelectrolysis, however, the thermal neutral voltage is also a function of gas composition. Figure 7 presents internal stack temperature depression (the difference between the temperature measured during the sweep and the temperature at open cell conditions) for thermocouple #2 as a function of stack operating voltage for the 7 electrolysis conditions listed in Table 1. By curve fitting the experimental data (shown as lines in Figure 6) and solving for zero temperature depression, experimental thermal neutral voltages were estimated. Experimental open cell potentials were directly measured. Theoretical open cell potentials were calculated using the chemical equilibrium model described above. Theoretical thermal neutral voltages were estimated by extending the chemical equilibrium coelectrolysis model discussed to include an energy balance. Table 2 summarizes the measured versus predicted open cell potentials and

TABLE 2. Comparison of measured versus predicted open cell potentials and thermal neutral voltages.

Test #	Open Cell Potential (volts per cell)		Thermal Neutral Voltage (volts per cell)	
	Measured	Predicted	Measured	Predicted
1	0.8795	0.8923	1.3004	1.3437
2	0.8959	0.9082	1.3231	1.3476
3	0.8700	0.8826	1.3271	1.3446
4	0.8392	0.8421	1.3017	1.3161
5	0.8696	0.8803	1.3447	1.3451
6	0.8376	0.8471	1.3265	1.3285

thermal neutral voltages for the experimental conditions listed in Table 1. The average difference between measured and predicted thermal neutral voltages for the 6 coelectrolysis tests conducted was 17 mV.

Figs. 8-13 present the steady state outlet compositions of steam, CO<sub>2</sub>, hydrogen, and CO as a function of electrolysis current on a dry basis for tests 1-6. Lines represent various model predictions and symbols represent experimental measurements. An in-line gas chromatograph was used to measure outlet compositions from the stack. Since the gas chromatograph requires a dry sample, the sampling location was downstream of the condenser to remove as much water from the sample as possible. The sample was passed through a dessicant as well. At this point, the sample gas stream is at approximately room temperature. As noted previously, the RSR equilibrium constant is a function of temperature, but will kinetically freeze below some temperature in the absence of the nickel catalyst. Therefore, it was not obvious what value to use for an “apparent” equilibrium temperature in the model for the products. Therefore, the chemical equilibrium coelectrolysis model was run for several different equilibrium temperatures ranging from 650°C to 800°C (Fig. 8). It was found that setting the chemical equilibrium coelectrolysis model equilibrium temperature equal to the furnace temperature produced the best comparisons, indicating that the products are kinetically frozen after they leave the hot zone, probably due to lack of any significant catalyst surface and the cool-down is fairly rapid. Predicted compositions were therefore evaluated at the electrolyzer temperature for all subsequent evaluations (Figures 9 through 13).

Figs. 8 through 13 demonstrate that even at zero current there was a drop in CO<sub>2</sub> and H<sub>2</sub> mole fractions from the cold inlet values, with CO produced. This is solely due to the RSR. As the electrolysis current was increased, the yield of syngas increased linearly while the concentration of CO<sub>2</sub> (and H<sub>2</sub>O, not shown in the figures) decreased. These figures also show overall good agreement between experimental GC data and results from the chemical equilibrium coelectrolysis model for the range of testing performed in this study. Finally, in the case of Test #6, at the maximum current studied the product H<sub>2</sub> concentration was doubled and product CO<sub>2</sub> concentration was reduced to half that of the process inlet mixture. Coelectrolysis significantly increases the yield of syngas over the reverse water gas shift reaction equilibrium composition.

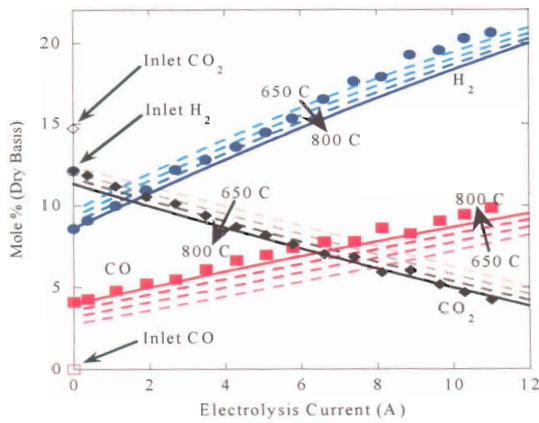


Fig. 8. Effect of varying chemical equilibrium coelectrolysis model equilibrium temperature (Eq. 9) with comparison to Test 1 experimental data..

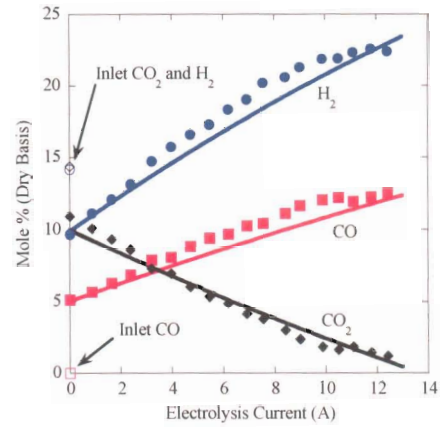


Fig. 9. Test 2 experimental and chemical equilibrium coelectrolysis model results,  $T_{equil} = 800$  C.

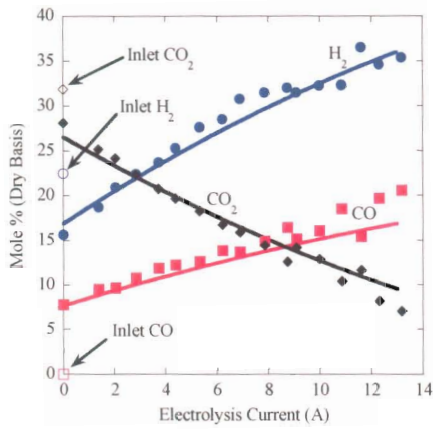


Fig. 10. Test 3 experimental and chemical equilibrium coelectrolysis model results,  $T_{equil} = 800$  C.

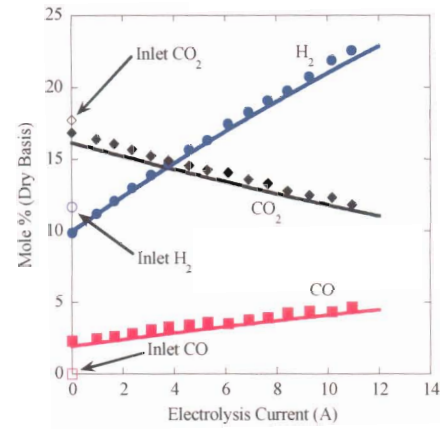


Fig. 11. Test 4 experimental and chemical equilibrium coelectrolysis model results,  $T_{equil} = 800$  C.

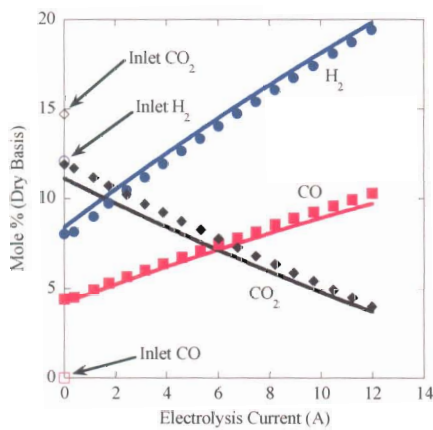


Fig. 12. Test 5 experimental and chemical equilibrium coelectrolysis model results,  $T_{equil} = 828$  C.

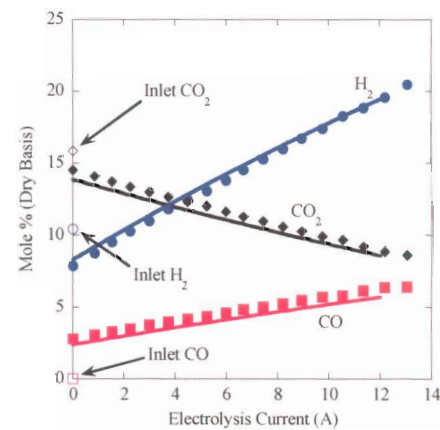


Fig. 13. Test 6 experimental and chemical equilibrium coelectrolysis model results,  $T_{equil} = 828$  C.

## V. CONCLUSIONS

Over the past three years, the INL has been actively evaluating high temperature coelectrolysis in solid oxide cells for large scale syngas production from a water / CO<sub>2</sub> feedstock. Results presented in this paper were obtained from a 10-cell planar electrolysis stack, with an active area of 64 cm<sup>2</sup> per cell. Inlet gas composition, electrical current, and stack operating temperature were varied. Stack apparent ASR values were shown not to vary significantly between pure steam electrolysis and steam / CO<sub>2</sub> coelectrolysis. Product gas compositions were measured via an online micro gas chromatograph (GC) and showed good comparison to predictions obtained from a chemical equilibrium coelectrolysis model developed at the INL. Results show that coelectrolysis significantly increases the yield of syngas over the reverse water gas shift reaction equilibrium compositions. Theoretical Nernst potentials and thermal neutral voltages for coelectrolysis also compared well to experimentally measured values. Better understanding of the feasibility of producing syngas using high temperature electrolysis may initiate the systematic investigation of nuclear-powered synfuel production as a bridge to the future hydrogen economy and ultimate independence from foreign energy resources.

## NOMENCLATURE

$a, b, c, d$	mole fractions CO, CO <sub>2</sub> , H <sub>2</sub> , and H <sub>2</sub> O respectively
$A_{cell}$	active area of each cell, cm <sup>2</sup>
$ASR$	apparent area specific resistance, Ohm cm <sup>2</sup>
$F$	Faraday's constant, 96487 J/V mol
$\Delta G_f$	Gibbs free energy of formation, J/mol
$I$	total electronic current, A
$k_{RSR}$	Reverse Shift Reaction equilibrium constant
$n$	number of measurements
$\Delta n_0$	relative molar rate of oxygen removal from the CO <sub>2</sub> /steam side, mol/s
$N_{cells}$	total number of cells in the stack
$\dot{N}_{Tot, fuel}$	total molar flow rate on CO <sub>2</sub> /steam side of cells, mol/s
$P$	pressure, Pa



$P_{std}$	standard pressure, Pa
$R$	universal gas constant, J/mol K
$T$	temperature, K
$V_N$	Nernst potential, V
$V_{OC}$	stack open cell potential, V
$V_{op}$	stack operating voltage, V
$y$	mole fraction

### ACKNOWLEDGMENTS

This work was supported by the Idaho National Laboratory, Laboratory Directed Research and Development program and the U.S. Department of Energy, Office of Nuclear Energy, Nuclear Hydrogen Initiative Program.

### REFERENCES

1. C.M. Stoots, J.E. O'Brien, G.L. Hawkes, J.S. Herring, and J.J. Hartvigsen, "High Temperature Co-Electrolysis of H<sub>2</sub>O and CO<sub>2</sub> for Syngas Production," *2006 Fuel Cell Seminar*, Honolulu, Hawaii, Nov. 13-17, 2006, paper no. 418.
2. G.L. Hawkes, J.E. O'Brien, C.M. Stoots, R. Jones, "Three Dimensional CFD Model of a Planar Solid Oxide Electrolysis Cell for Co-Electrolysis of Steam and Carbon-Dioxide," *2006 Fuel Cell Seminar*, Honolulu, Hawaii, Nov. 13-17, 2006, paper no. 298.
3. S.H. Jensen, J.V.T. Høgh, R. Barfod, M. Mogensen, "High temperature electrolysis of steam and carbon dioxide," In *Energy technologies for Post Kyoto targets in the medium term*, Proceedings of *Risø International Energy Conference*, Risø, Denmark, May 19-21, 2003.
4. S. H. Jensen, and M. Mogensen, "Perspectives of High Temperature Electrolysis Using SOEC," *19<sup>th</sup> World Energy Congress 2004*, Sydney, Australia, September 5-9, 2004.
5. J.E. O'Brien, C.M. Stoots, and J.Hartvigsen, "Hydrogen Production Performance of a 10-Cell Planar Solid-Oxide Electrolysis Stack," *Journal of Fuel Cell Science and Technology*, **3**, 1 (May 2006).